

Ing. Tomáš Ščepka

Autoreferát dizertačnej práce

**NONINVASIVE CONTROL OF MAGNETIC STATE IN FERROMAGNETIC NANODOTS
BY HALL PROBE MAGNETOMETRY**

**NEINVAZÍVNE VYŠETROVANIE MAGNETICKÉHO STAVU VO FEROMAGNETICKÝCH
NANOOBJEKTOCH POMOCOU HALLOVEJ MAGNETOMETRIE**

na získanie vedecko-akademickej hodnosti *philosophiae doctor*

v doktorandskom študijnom programe: **Fyzikálne inžinierstvo**

v študijnom odbore: 5.2.48 Fyzikálne inžinierstvo

Bratislava 2016

Dizertačná práca bola vypracovaná v dennej forme doktorandského štúdia

Na Elektrotechnický ústav, Slovenská akadémia vied
Dúbravská cesta 9, 841 04 Bratislava

Predkladateľ: **Ing. Tomáš Ščepka**
Elektrotechnický ústav, SAV
Dúbravská cesta 9, 841 04 Bratislava

Školiteľ: **RNDr. Vladimír Cambel, DrSc.**
Elektrotechnický ústav, SAV
Dúbravská cesta 9, 841 04 Bratislava

Oponenti:

Autoreferát bol rozoslaný dňa:

Obhajoba dizertačnej práce sa koná dňa o hod. pred komisiou pre obhajobu dizertačnej práce v odbore doktorandského štúdia 5.2.48 Fyzikálne inžinierstvo, vymenovanou predsedom spoločnej odborovej komisie na Elektrotechnickom ústave SAV, Dúbravská cesta 9, v zasadačke ústavu.

.....

prof. Dr. Ing. Miloš Oravec
Dekan FEI STU
Ilkovičova 3, 812 19 Bratislava

1	INTRODUCTION	1
2	GOALS OF DISSERTATION THESIS	2
3	MAGNETIC STATES IN FERROMAGNETIC SUB-MICRON DOTS	3
4	EXPERIMENTAL PART – FABRICATION AND MEASUREMENTS	5
	4.1 Preparation of Hall Microprobes	5
	4.2 Preparation of Magnetic Particles	6
	4.3 Vortex dynamics in a 1 μm PL micromagnet	7
	4.4 Individual vortex nucleation/annihilation in a 300 nm PL nanomagnet	10
5	CONCLUSIONS	19
6	ZÁVER	20
7	PUBLICATIONS AND PRESENTATIONS	21
8	REFERENCES	22

1 Introduction

The motivation for this work lies primarily in the need to design and fabricate miniaturized ferromagnets that could be utilized as units in magnetic storage devices. All digital devices have bits stored in certain form (up and down, on and off). For magnetic media, it is usually in the form of grains where all the spins are aligned. The higher areal density means more bits in the same region, however, such an increase in the number of bits is only possible until the thermal vibrations are still negligible. As the superparamagnetic limit restricts the areal densities, scientists are still looking for new ways how to encode binary information. Magnetic vortex cores that are of small enough dimensions and thermally stable could offer one promising candidate. However, an application of memory cells in storage devices requires a high stability of a memory state, a high repeatability of read/write cycles and uniformity of the switching fields for different, but nominally identical nanoparticles. It means that magnetization reversal has to take place in a well-defined manner.

The topic of the vortex dynamics involves both the reading mechanism and the ways how to write the desired information. The writing process in our experimental work is based on the excitation with a magnetic field. The important parameters in the magnetic switching process are vortex nucleation and annihilation fields. These fields as well as magnetisation configurations depend on the temperature and direction of an applied magnetic field.

Micro-Hall magnetometry offers advantages compared to other diagnostic techniques. For example, it provides sufficient sensitivity to examine single nanoparticles without influencing their magnetic behavior during the experiment. In addition, a sufficient lateral resolution, which is limited by the minimal width of the active area can be achieved. Operated in the ballistic transport regime, Hall sensors can be used to perform quantitative measurements of the stray field over a wide range of temperatures and external magnetic fields.

In the thesis we review our achievements in this research field with a particular interest in submicron ferromagnetic dots with broken symmetry, for which Permalloy has been chosen as the material. The considerable focus is given to the vortex dynamics due to excitation with a magnetic field. The study of vortex nucleation and annihilation processes and their temperature dependences in sub-micrometer-sized Pacman-like ferromagnets followed.

At the end of this work we should be able to confirm whether it is possible to control magnetic states in the Pacman-like ferromagnets by an applied in-plane magnetic field and whether the realized micro-Hall magnetometry has a potential to observe these states.

2 Goals of Dissertation Thesis

Within the scope of this thesis, the following tasks have been performed:

- Develop a technology of micro- and sub-micrometer Hall probes based on a GaAs/AlGaAs heterostructure with ferromagnetic (Permalloy) object of various shapes – lowered symmetry (Pacman-like) nanomagnets.
- Identify magnetic states in Pacman-like nanoobjects by means of the micro-Hall magnetometry and design a mechanism how to control the chirality and polarity of particular nanomagnets.
- Analyse the magnetic behaviour in nanoobjects in relation to the temperature and magnetic field direction and compare the results obtained from measurements with calculations, eventually with other nanoobject shapes.

Additional subtasks to meet the desired goals:

At the earliest I had to learn the Hall probe micromachining that has a long tradition at our institute. Then, since we have employed different heterostructures, it has been necessary to find suitable etching parameters for each of them. The Hall probe micromachining includes the study of etching times, etching ratios, and related structure profiles. In the next step my focus has been directed to SEM observations and the EBL lithography. Here, two major tasks have been considered, a Hall probe downscaling and ferromagnet fabrication. Much effort has been expended in EBL structure testing that includes activities such as dose and pattern tests, studying of the influence of the exposed material, varying lift-off parameters, and so on. Scaling down the ferromagnet size meant to use slightly different approaches. The exact location of the nanoobject on the border of the HP's sensing region has been also a tricky task that has required a considerable effort. Besides, the ohmic contact formation and ways, how to improve the bonding process, have been examined.

After the sample preparation, further tasks have been focused on the system designed for magnetic measurements where the sample placement has represented a critical point. The modification of the sample holder helped us to investigate samples in a desired manner. All other procedures have dealt with magnetic measurements and their evaluation. While a sample has been exposed to an external magnetic field, parameters such as a direction and magnitude of the field, temperature, sweeping speed, current through a probe, relaxation time, have been changed and tested.

3 Magnetic States in Ferromagnetic Sub-Micron Dots

The magnetisation reversal process has been investigated with integral methods on arrays of disks, for example, by using the magneto-optic Kerr effect [1] and Brillouin light scattering [2], and on individual particles by employing micro-superconducting quantum interference device and micro-Hall magnetometry [3]. From such experiments, it is clear that the magnetisation reversal of magnetic particles involves vortex formation, propagation, and annihilation. However, the detailed mechanism of these events is still unrecognized and thus it is an open problem.

The following experiments have mostly used micro-Hall sensors fabricated from GaAs/AlGaAs heterojunction material to measure stray field hysteresis loops of individual particles [4]. Works presented here are focused on the single-particle observations while a static magnetic field is applied to initialize the magnetic reversal. Different shapes of ferromagnets are considered, from circular nanodisks to objects with broken symmetry.

The stray field occurring during magnetisation reversal in a magnetic nanodot is significant and may have an impact on the micromagnetic behaviour of neighbouring magnetic elements or on the sophisticated multilayer devices. The reversal depends on the particle's diameter, nanodots with diameter $d \leq 100$ nm show bistable switching while more complex behaviour is occurred for diameters $d > 300$ nm.

Memory effects in individual submicrometer ferromagnets were observed by Lok, Geim, and others in 1998 [5]. They studied the magnetisation of individual nickel disks (80 nm high, $d = 0.1 - 1$ μm) at low temperatures. In their experiments the hysteresis loops of the nickel disks did not show inversion symmetry at temperatures below 19.8 K and did so for higher temperatures. Furthermore, they found out that the magnetisation of the disks with diameter $d = 0.1 - 0.2$ μm can be frozen into two possible states. For such a low temperature these two states are very stable, while at slightly higher temperatures a 100x lower field (100 mT) can fully polarize the disks. Further, they observed that the amplitude of the magnetisation signal increases quadratically with increasing disk diameter.

In 2001 Hengstmann with his group measured the stray field of individual nanostructured Permalloy disks by means of sub- μm Hall magnetometer (Hall probe width ~ 500 nm, electronic width ~ 300 nm) [6]. They investigated circular nanomagnets with diameters of 500-700 nm and thickness of 20 nm. Their experimental Hall curves indicated that the disks are in the vortex phase near remanence and an averaged value of the stray field of 36 mT was measured in the 700 nm disk (23 mT in the 500 nm disk) at 4.2 K while the external magnetic field was swept between ± 150 mT. It was also found that the saturation field decreases with an increase in the diameter of the nanodisk.

Rahm and his colleagues investigated both experimentally and by means of micromagnetic calculations magnetic states preceding vortex formation in Permalloy nanodisks ($d = 500$ nm, $t = 40$ nm) in 2003 [7]. They observed both from calculations and experiments that the vortex formation can be reached via different states. They showed that the formation of the patterns (both s- and c-state) can be accompanied by discontinuous deformations of the pre-vortex spin structure as a function of the external field [8].

In the following years a lot of scientists have studied different shapes of ferromagnets with broken symmetry that would allow an easy magnetic control. Even though it was not experimentally proved, the authors in Ref. [9] investigated the static and dynamic magnetisation reversal process in ferromagnetic sub-micron dots with lateral gradient magnetisation. The simulations showed that the sub-dot with lateral gradient magnetisation produces a two-stage magnetisation reversal during nucleation.

In Ref. [10] they investigated the arrangement effects of triangular defects on the magnetisation configurations and switching process of a Permalloy disk ($d = 250$ nm, $t = 25$ nm) by micromagnetic simulations. Introduction of the shape anisotropy to the defect produces a change of the magnetostatic energy, and then it may mediate reversal process of the disk. They showed the strong correlation of the nucleation field and the chirality of the vortex with the orientation of the triangular defect.

In order to investigate the temperature dependence of the critical fields in ferromagnets, the measurements of large arrays of disks (submicron square Py structures [11] or sub-100 nm Fe disks [12]) have been performed [13]. Since they reflected a statistical average of reversal modes of individual disks, it prevents more detailed insight into the magnetisation reversal process. These dependences could reveal the problem of energy barriers between the vortex state and uniform single-domain states and other important features arising from thermal effects. One of the papers that represented incentives in our study, was a work by Mihajlovic et al. dealing with temperature dependent nucleation and annihilation of individual magnetic vortices investigated by means of micro-Hall (Figure 3-1) and bend-resistance magnetometry [14]. They studied different sizes of Py disks ($d = 520 - 865$ nm, $t = 50$ nm) and were able to identify thermal effects in the smallest and largest disks. They found out that at low temperature vortex nucleation and annihilation proceed via thermal activation over an energy barrier, while at high temperatures they are governed by temperature dependence of the saturation magnetisation of the disk.

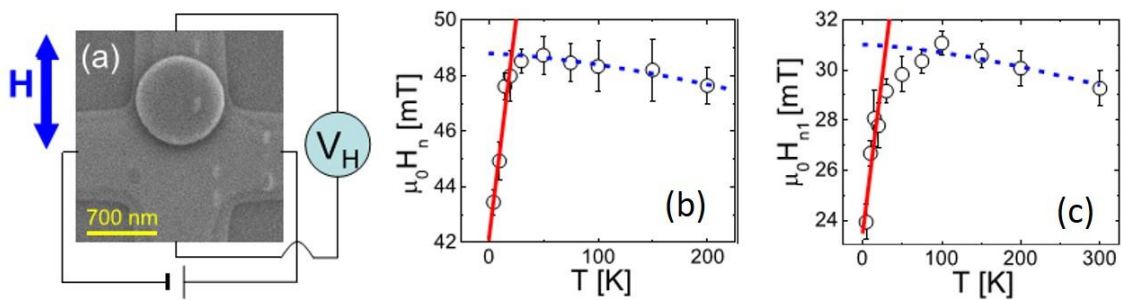


Figure 3-1 (a) SEM micrograph of a Hall cross with 865 nm Py nanodisks measured in micro-Hall configuration. Double-sided arrow indicates directions of an applied magnetic field. (b) Temperature dependence of the nucleation field for 526 nm disk measured with band-resistance magnetometry. (c) $H_n(T)$ dependence for 865 nm disk measured with μ -Hall magnetometry. Both characteristics show two different slopes [14].

The results showed variations in both critical fields. Especially, vortex nucleation field H_n exhibited a two-slope behaviour with a sharp increase for temperatures up to 50 T and slow decrease above it. They described this mechanism as a thermally activated vortex nucleation over an energy barrier for temperatures below ~ 50 T and as the decrease in the saturation magnetisation of the disk due to thermally excited spin waves for higher temperatures (Figure 3-1b and c).

The vortex state in submicron dots is stable and this stability has a potential as a unit cell for high density magnetic storage and magnetic logic devices. A key issue is to understand and control the magnetic reversal of the submicron dots. Considering the stability of devices, which are based upon a single domain state in zero applied field, it could be shown that a single domain state at remanence is not a sufficient criterion for the usage of a specific element in a device, but an appropriate shape anisotropy is crucial. If the shape anisotropy is too small, magnetic vortices can be formed by magnetic stray fields which exceed a specific critical value, and the stored information is destroyed by the created vortex. Such unwanted stray fields may arise during the writing process of neighbouring bits in magnetic data storage devices.

4 Experimental Part – Fabrication and Measurements

In this part I present my own results in micromagnetism and nanomagnetism that I obtained at the Institute of Electrical Engineering, Slovak Academy of Sciences in Bratislava. Individual sections are focused on the fabrication of Hall probes and ferromagnetic nanomagnets. Magnetisation reversal processes and other magnetic effects in nanomagnets are placed under scrutiny.

4.1 Preparation of Hall Microprobes

The micro-Hall magnetometry offers a way to study the magnetic properties of individual particles over a wide range of temperatures in the presence of strong external magnetic fields. As we also noticed in our experiments, the operational range of 2DEG Hall micro-sensors is not limited to low temperatures, but their sensitivity rapidly worsens at temperatures above 100 K. It is mainly because of a rapid increase in low-frequency resistance fluctuations [15].

The fabrication includes the patterning of a micron-sized cross junction into a semiconductor heterojunction material containing a two-dimensional electron gas under its surface. This definition is usually done by optical lithography followed by wet chemical etching. One path of this Hall cross is used to carry the current, whereas the other one serves as a voltage probe.

The structure consists of 300 nm buffer, 20 nm Al_{0.3}Ga_{0.7}As spacer, delta-doped Si-layer, 50 nm Al_{0.3}Ga_{0.7}As top layer, and 5 nm GaAs cap layer (Figure 4-1). The Al_{0.3}Ga_{0.7}As/GaAs heterostructures contained a 2DEG approximately 80 nm below the surface. Delta-doped layer was prepared during 30 second growth interruption in arsine overpressure.

Typical Hall sheet concentrations for identical structures were $9.6 \times 10^{11} \text{ cm}^{-2}$ and Hall mobility was about $5000 \text{ cm}^2 \text{ V}^{-1} \text{ s}^{-1}$ at room temperature and $86\,000 \text{ cm}^2 \text{ V}^{-1} \text{ s}^{-1}$ at 4.2 K.

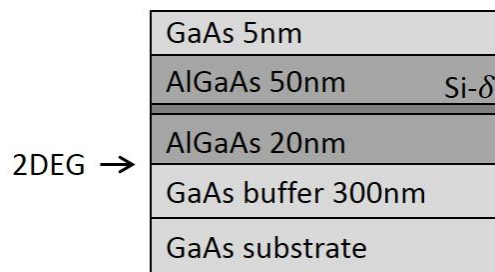


Figure 4-1 Schematic of the initial heterostructure with the 2DEG for HP micromachining.

The structure is etched by means of wet chemical etching in a H₃PO₄:H₂O₂:H₂O solution with the ratio 1:2:8 for 20 s. The etch depth should be about 375 nm, since we want to interrupt the 2DEG as well as the whole buffer layer. After the etching, remaining photoresist is removed by standard lift-off using acetone followed by water rinse.

Hall Probe Downscaling

After the formation of 15 μm Hall crosses, their further miniaturizing is needed to obtain local magnetic information. Electron lithography along with wet chemical etching (1:2:8 H₃PO₄:H₂O₂:H₂O, 10 s) is utilized to prepare a miniaturized 1- μm -wide cross. This results in a very limited pathway of charge carriers under the cross surface. It is also necessary to note that the edges of the cross structure are depleted, thus the real width of carrier pathway is reduced to somewhere between 750 and 900 nm.

Hall Probe Contacts

In order to connect and measure the fabricated Hall crosses, contact metals have to be deposited. The contact mask is used to pattern a structured surface lithographically. The exposition and developing process are the same as it was described earlier for the photoresist. The contact metals are prepared by sequential deposition of Ni, AuGe, Ni onto a clean GaAs/AlGaAs heterostructure [16]. This ternary metal is well established in our group. The Ni overlayer is added in order to maintain a smooth surface morphology after alloying the contact metal and the bottom Ni layer improves adhesion between the metal and the GaAs material and leads to more uniform contact resistances. All layers are deposited by thermal evaporation in the AJA Orion 8E evaporation system. After the deposition, a rapid thermal annealing of the sample under N₂ at 450°C for 40 s is applied to form ohmic contacts. The resistance values between the opposite contacts ranged from 1 to 3 kΩ.

4.2 Preparation of Magnetic Particles

It is obvious that in order to find appropriate parameters for e-beam exposure, dose tests have been done in advance. Usually two parameters have been altering in the dose tests: nanomagnet pattern size and exposing dose. In the initial tests different patterns have also been used to achieve an ideal PL nanomagnet.

Scanning electron microscopy is used to check the size and shape of micro/nanomagnets. Figure 4-2 shows a just deposited 2-μm PL micromagnet on a GaAs surface. Such a large object is possible to fabricate with high success. The opening is exactly as big as we wanted and the edge distortion is not significant. Although it is quite simple to make such particles in terms of technology, we do not have any idea what magnetic state can be trapped inside and it is a reason why further downscaling is needed.

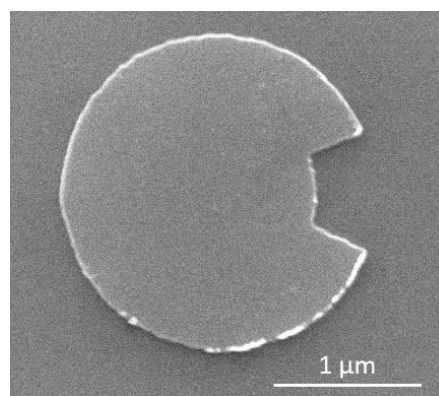


Figure 4-2 A deposited 2-μm PL micromagnet keeps a proposed shape.

It is well established that PMMA lithographic processes have a maximum spatial resolution of 5–10 nm, due partly to the size and radius of gyration of the PMMA molecules. Furthermore, the intrinsic grain size of the deposited Permalloy may also limit the lithographic edge definition. The edge definition of the experimental particles can thus be no better than approximately 10 nm. These limitations, however, are far behind our considered nanomagnets. Based on our simulations it is preferred to have ferromagnets with diameter below 100 nm, specifically 70 nm. Although it is not possible to fabricate these structures on a GaAs material in our laboratory at the moment, the simulations reveal that the magnetic states may be also reliably determined for the PL objects a little bit smaller than 350 nm.

As a matter of fact, the smaller particles, the weaker signal recorded. Thus, it is often necessary to measure arrays of nanomagnets in order to obtain a sufficiently large signal. The high definition of the lithography means that all of the particles in the array are virtually identical to each other and so the measured properties for an array can also be interpreted as the individual properties of a single nanomagnet. It is not our situation and we do not have to average the signal. We are lucky in our study because we measure individual properties of a single particle (300 nm) by means of micro-Hall magnetometry and we still receive sufficient signal.

4.3 Vortex dynamics in a 1 μm PL micromagnet

At first, we tested ferromagnetic objects with a diameter of about 1 μm . In particular, we studied Pacman-like magnets, which are mentioned earlier in a more detail. Even though the simulations performed had been related to the much smaller diameters, one of our first objectives has been to find out the magnetisation behaviour in the PL micromagnets under certain conditions, such as low temperatures, direction and magnitude of an applied magnetic field.

Figure 4-3 shows a fabricated micro-Hall probe with a PL micromagnet located directly on the probe. Only one PL object was patterned per cross to enable single domain observation. The active region of the probe is approximately $1 \times 1 \mu\text{m}^2$. The PL micromagnet is shifted from the central position to improve the measured signal. In our case the best resolution is achieved for the so-called Hall configuration when current flows between leads I+ and I-, and a voltage drop is measured between leads V+ and V-.

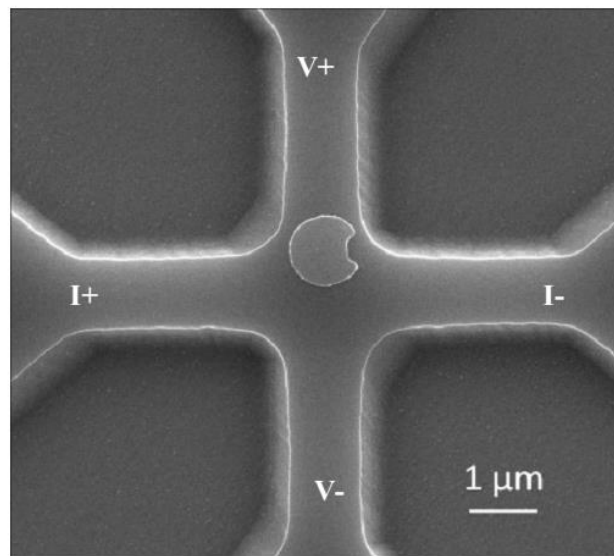


Figure 4-3 Scanning electron microscope micrograph of a miniaturized Hall probe with a Pacman-like micromagnet (diameter of 1 μm).

Measurements were carried out at temperature of 77 K. Generally, we have applied dc current of 10 (20) μA and the Hall voltage was measured at the remaining, opposite arms of the cross (there exists also the Band resistance configuration, where a voltage drop is measured at the neighbouring arms of the Hall cross). For magnetisation reversal measurements, a homogeneous magnetic field was applied in the plane of the ferromagnet.

To confirm magnetisation curves from our experimental results, the simulations have been performed on a 1- μm element that contains similar boundary defects as the fabricated PL micromagnet. Magnetic field in the simulation has been applied at the close angle with respect to the x-axis in the experiment. The magnetisation reversal curves (Figure 4-4b) have been simulated at zero temperature. All important points are labelled by letters (a-f) and for each point corresponding magnetic state is depicted in the Figure 4-6. The sequence illustrates reordering of the magnetic pattern while the external magnetic field is swept from saturation (a) to saturation with the opposite magnetisation (f) across the zero value. At 21 mT (b) vortex nucleates, the biggest jump at 6 mT (c) correspond to jump of the vortex to the central position. For the interval between 6 mT and -67 mT the vortex propagates perpendicular to the applied magnetic field. The annihilation of the vortex appears at -67 mT and afterwards the saturation is obtained.

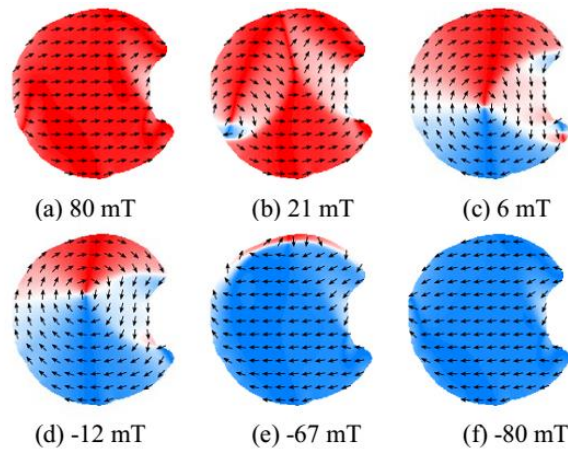


Figure 4-6 Simulation of local magnetic state within a PL micromagnet at certain values of an applied in-plane magnetic field.

Although we have obtained magnetisation reversal curves both experimentally and in the simulations, we are not able to make an exact conclusion about vortex dynamics (chirality orientation included) in a 1- μm PL micromagnet due to its complexity and further downscaling is necessary.

In addition, we have investigated a spot of the vortex nucleation for different angles of an applied magnetic field. The simulated results have shown that there is no specific defect which would help the vortex to enter the structure (Figure 4-7).

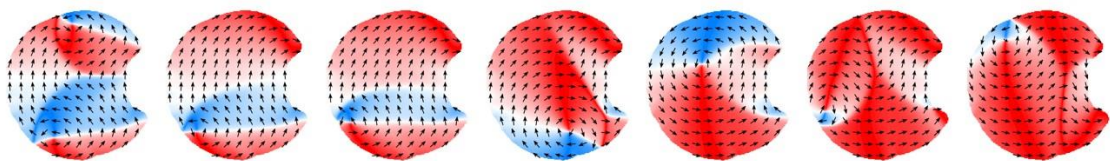


Figure 4-7 Nucleation spot examination. External in-plane magnetic field varies in relation to PL symmetry axis from left to right as follows: 90°, 75°, 60°, 45°, 30°, 15°, and 0°.

Similar angular study have been performed in order to define a ground state of the ferromagnet. The simulation started at 100 mT and the field value has been lowering until it reaches the zero field. At 0 mT, a magnetic state has been recorded.

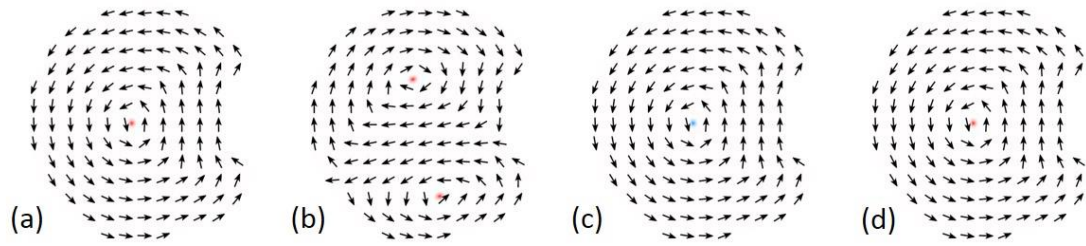


Figure 4-8 Magnetic states at 0 mT for different field angles: (a) 90°, CCW chirality, polarity+, (b) 60°, double-vortex, CCW/p+ and CW/p+, (c) 30°, CCW, p-, (d) 0° CCW, p+.

From the results mentioned above, one can see that angular dependence in the investigation of PL ferromagnets is necessary. Furthermore, unwanted complex states (double-vortex state) are present in the ferromagnetic objects with sizes over 350 nm.

4.4 Individual vortex nucleation/annihilation in a 300 nm PL nanomagnet

We came to a significant point of our work when we have reduced the diameter of PL ferromagnets. After the examination of objects at micrometre scale, we have focused our effort on the PL objects with the diameter below 350 nm. By this approach it has been possible to control magnetic states much easier and thus we could investigate other functionalities, such as temperature and angle dependences.

We have proceeded similarly as in the previous study. At first, micromagnetic simulations of the ideal PL magnet have been performed. These simulations suggested what could be expected in such a small object. Then, we have chosen the best looking objects from the fabricated nanomagnets and have studied their magnetization characteristics in external magnetic field and at various temperatures. Finally, to complete our study, simulations of the particular close-to-reality PL shape have been performed.

Since our aim is the single object examination, always only an individual particle has been placed on the Hall cross. Figure 4-9 shows one of the selected systems that has been used in the magnetisation reversal measurements. In addition to the desired shape of the ferromagnet, vertical profiles of the system (the height of the PL nanomagnet and Hall cross structure) have been measured by an AFM to determine the suitability. The working operation of the cross has been evaluated in a standard mechanical probe station.

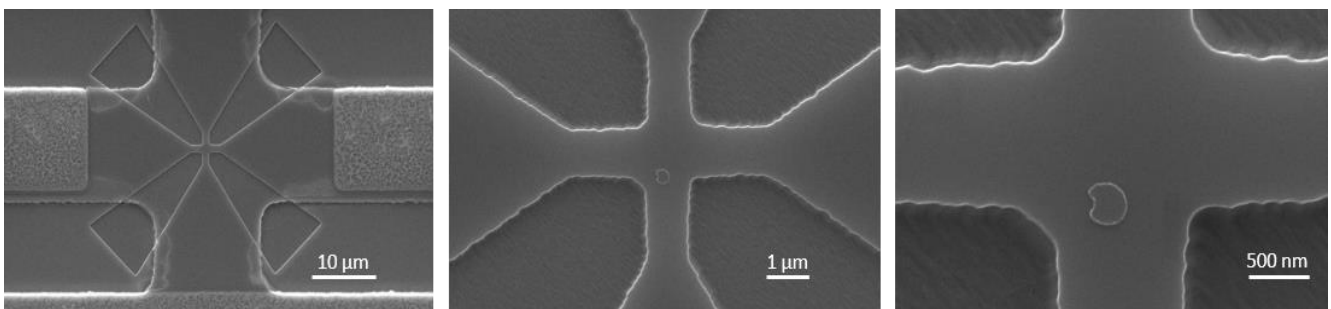


Figure 4-9 Selected system consisting of the miniaturized Hall probe and 300-nm PL ferromagnet. From left to right, a zoom-in sequence of the system.

Although we have not known the exact border of the active region in the Hall cross, we have assumed that the centre of the PL particle is placed somewhere close by. It means the sensitive region captures only a part of the PL stray field and thus a change of the signal recorded is more distinguished. To better

understand a distribution of the stray field from the PL nanomagnet, the maps of relative values of the z -component of the magnetic field have been calculated (Figure 4-13).

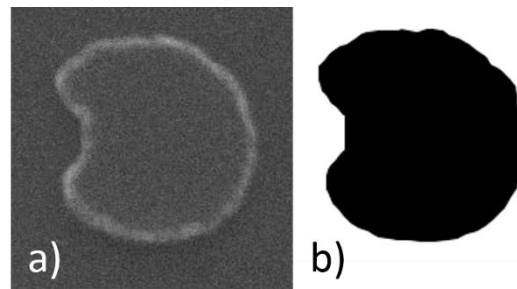


Figure 4-10 (a) a fabricated 300-nm PL nanomagnet, (b) an object used in the simulations containing similar boundary imperfections as in (a).

After the whole fabrication process, the sample has been placed into a Physical Property Measurement System (PPMS) sample chamber. At the bottom of the sample chamber is a connector pre-wired to the system electronics. This connector allows to plug in a removable sample insert or sample “puck” and offers convenient access to electrical leads for application hardware and electronics.

Since our PPMS is configured with a longitudinal magnet and we have not had any vertical puck adapter the situation has been a bit more complicated. It means that if we wanted to apply an in-plane magnetic field, we would have to make an adapter which places a sample in the vertical orientation. It has been simply done by a non-magnetic vertical stand being situated on a standard ACT puck. The sample has been then glued by a low-temperature glue on the stand. Bonding process of the sample to the puck has thus become more complicated. In addition to the issue mentioned above, we have just assumed that a magnetic field (in our specific distance from a standard position due to the vertical replacement) has similar parameters.

Hall measurements were carried out at temperatures between 4 K and 150 K. The amplitude of the current through the Hall probe was kept constant at either 10 μA or 20 μA , while the voltage drop was measured in the PPMS system (Figure 4-11). The voltage noise lower than ~ 20 nV has been achieved in the best case (integration time 10 s, $T = 30$ K). In order to obtain a full hysteresis loop of a nanomagnet, an external magnetic field, generated by superconducting coils, was applied in parallel with the Hall sensor surface and the direction of current flow.

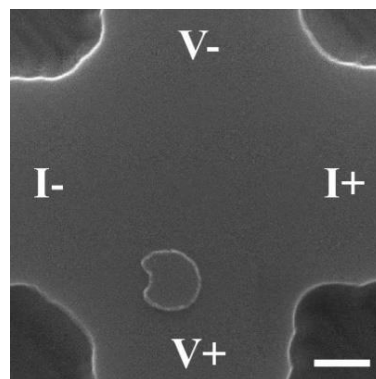


Figure 4-11 SEM micrograph of the PL nanomagnet placed asymmetrically on the active region of the micro-Hall probe. Connecting leads indicate the Hall configuration, where the current flows directly. Bar corresponds to 300 nm.

In the case of the 300-nm PL object our calculations have identified three different single domain (SD) states for field closely above the vortex nucleation: C-state, S-state, and double S-state. The pre-state influences the vortex nucleation process, which is with a high probability controlled by thermal activation over an energy barrier. The process is also influenced by the object asymmetry, which can be represented by additional magnetic dipoles located within the object at its boundary imperfections. Such dipoles change their value and direction during the magnetisation reversal measurements. The charge rearrangement should be sensitive also to thermal processes and represents small energy barriers for the vortex nucleation process.

The Hall voltage measured is proportional to the average magnetic flux through the active region of the probe generated by PL nanomagnet. The sweeping amplitude of the external field has been fixed at 2 T, for which the system reaches saturation and thus both the positive and negative branches of the hysteresis loop gave the same fields H_{nuc} (H_{an}). This has not been the case for applying fields of lower amplitudes (200 mT), probably due to boundary defects of the PL nanomagnet. Only sufficiently high external magnetic field brings the object into identical SD states for both field polarities.

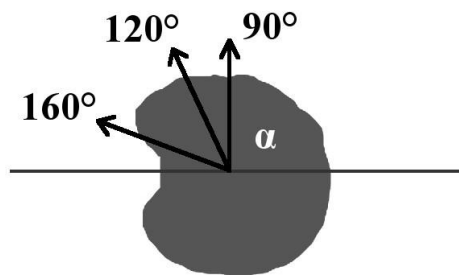


Figure 4-12 Three angles (α) of the applied magnetic field with respect to the PL nanodot. Horizontal line represents its symmetry axis.

We have analysed the vortex nucleation/annihilation process for three different field orientations, 90°, 120°, and 160° according to its symmetry axis (Figure 4-12, Figure 4-13). These angles have been selected based on the outputs of micromagnetic simulations and should represent robust states. The OOMMF software solves the LLG equation and simulates experiment at 0 K. At first, we have calculated the angular dependence of the SD-to-vortex state transitions, H_{nuc} and H_{an} . The calculations have shown three distinct configurations of local magnetisation in the PL nanomagnet.

In the Figure 4-13, line 1 shows simulated magnetisation states for the external field value just above the vortex nucleation field H_{nuc} – for field angle $\alpha = 90^\circ$ (C-state, left column), for $\alpha = 120^\circ$ (S-state, middle column), and for $\alpha = 160^\circ$ (double S-state, right column). Red curves highlight the current magnetic single-domain state. Line 2 and 3 depict the map of relative values of the z -component of the PL stray field at the 2DEG distance. Line 2 and line 3 shows the magnetic state before and after nucleation, respectively. Two colours correspond to two field stray polarities – blue for the negative and red for the positive z -component of the magnetic field. Dashed lines represent the border of the active region and thus area above the line is considered as sensitive region of the probe. Line 4 shows a z -component map at the distance of 10 nm from the PL nanomagnet. Stray fields near the PL opening are strong enough in the both cases, at the distance of 2DEG and 10 nm below the HP surface. From these maps one can easily define the vortex chirality (clockwise, CW, for left column; counter-clockwise, CCW, for the remaining columns).

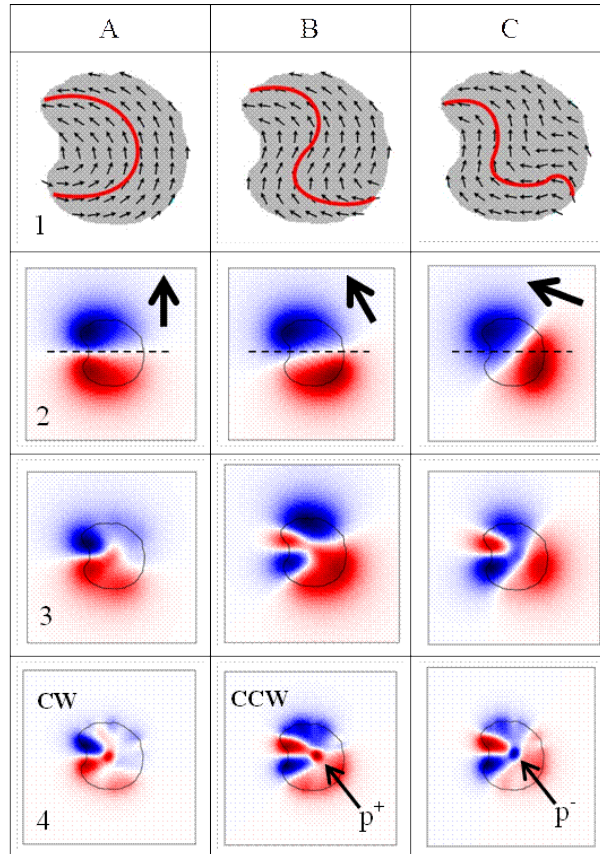


Figure 4-13 Three distinct pre-nucleation configurations of the magnetic state. Column A is for field angle $\alpha = 90^\circ$, column B for $\alpha = 120^\circ$, and column C for $\alpha = 160^\circ$. Arrows indicate direction of an applied field. Line 1: Field higher than H_{nuc} , three different single-domain states, C-state for $\alpha = 90^\circ$, S-state for $\alpha = 120^\circ$, and double S-state for $\alpha = 160^\circ$. Line 2: z -component of the stray field that corresponds to states shown in line 1 at the distance of 2DEG. Line 3: Field lower than H_{nuc} , z -component of the stray field at the distance of 2DEG. Stray field is strong at the PL's opening and defines clearly vortex chirality - vortex polarity is not so clear. Line 4: the same like line 3, but only 10 nm from the object – vortex chirality (CW, CCW) and polarity (p^+ , p^-) are clearly seen in the object.

On other hand, it is quite tricky to define the vortex polarity at the 2DEG distance. However, when we move closer to the surface, at the distance of 10 nm, the vortex polarity can be much better recognized. In the figure we can also find a dependence between the pre-nucleation state and the vortex state. The vortex state nucleated from a C-state differs from the one from an S-state in chirality, and vortex states created from an S-state and a double S-state differ in polarity. The calculations show that the chirality contribution to the Hall signal is about 20%, while the vortex polarity contribution is about 10 times smaller and thus considered as on the noise level at the 2DEG level.

As previously mentioned, the PL shape and the vortex polarity/chirality influence the magnetisation reversal signal. Figure 4-14(a) and (b) show magnetisation reversal curves for the field angle of 90° at 30 K. Abrupt changes in the stray field correspond to significant changes of the magnetisation, resulting in the step change of the system or its redistribution between the exchange and magnetostatic energy. While smooth changes in the signal are generated by the transformation of the magnetisation patterns.

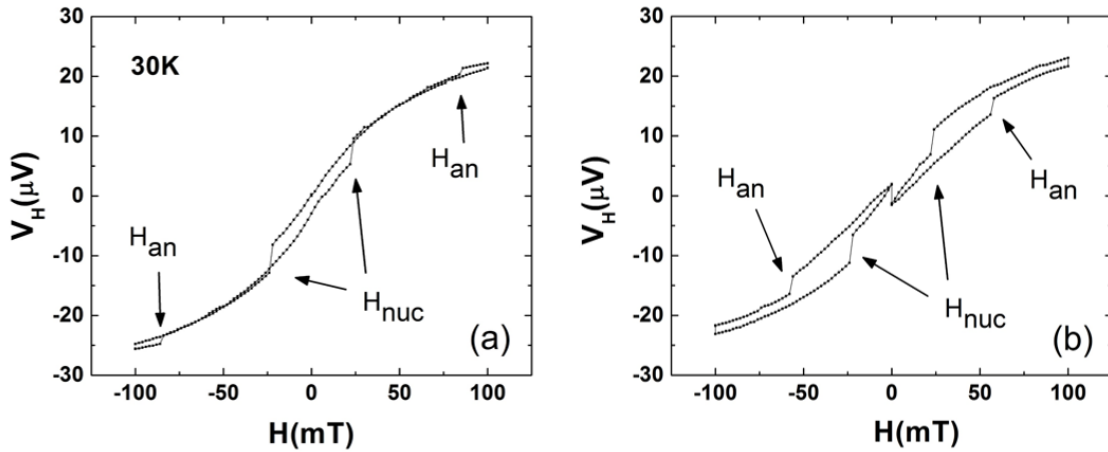


Figure 4-14 Hysteresis loops (V_H vs. H) for $\alpha = 90^\circ$ (C-state), $T = 30\text{ K}$. (a) annihilation of the vortex at a spot opposite to the PL opening. (b) annihilation at the PL opening. The loop is constructed of two curves.

Unlike a disk, the Hall signal from the PL nanomagnets depends significantly on the vortex chirality and can be easily controlled by the time sequence of the applied magnetic field. Figure 4-15 depicts the time sequence used to set a desired chirality of the vortex state in a particle.

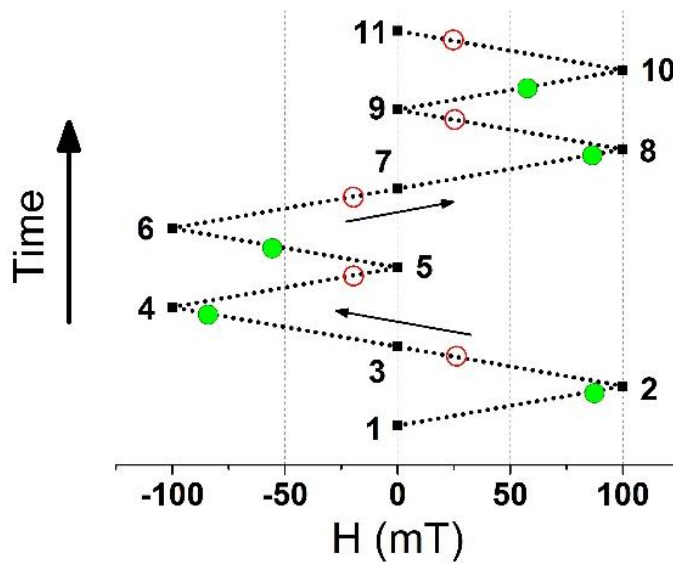


Figure 4-15 Time/field sequence of the nucleation (empty red points) and annihilation (full green points) events. The applied field is gradually swept from 1 to 11. Time scale is ~ 1 hour.

The time sequence works as follows:

Starting from the point 1 at zero field and with the CW chirality. In the next step, the positive field of +2 T is applied and recorded only up to +100 mT (point 2). The first annihilation event is occurring at $H_{\text{an}} = 88\text{ mT}$ on the right side of the object (Figure 4-16, inner red arrow). After the saturation, the field value is lowered gradually until the nucleation of the vortex is occurred. This event is represented by a red circle at $H_{\text{nuc}} = 25\text{ mT}$ and the chirality is set to CCW [17]. Negative field then expels the vortex core to the right side again due to the CCW chirality, and the vortex annihilates at $H_{\text{an}} = -88\text{ mT}$. The field value is further increased until the saturation state with the opposite direction of magnetisation is obtained

(-2 T). Heading back to the zero field state, another nucleation happens at $H_{\text{nuc}} = -22.5$ mT with the CW chirality. That means there is a different chirality between points 1-2 and 2-3, while the chirality in points 1 and 3 is the same. The vortex core is thus expelled only to the right boundary of the PL object (sequence 1-2-3-4-5, Figure 4-14a). We have cycled the sequence many times and we can conclude that all annihilation events occur at very similar field values, what proves that the vortex chirality is perfectly controlled in our experiments.

Now, the question is: Can we expel the vortex core to the left side of the PL object? We know, that by cycling the field from 0 T \rightarrow +2 T \rightarrow -2 T \rightarrow 0 T, never achieve an annihilation at the PL opening. However, if we reverse sweeping in the point 5, the vortex with the CW chirality will annihilate at $H_{\text{an}} = -56$ mT, followed by the nucleation at $H_{\text{nuc}} = -22.5$ mT with the same chirality. Such a half-loop (points 5-6-7) is depicted in the left part in the Figure 4-14b. Similar situation is for the positive half-loop (9-10-11), in which the CCW chirality is set and the vortex core is expelled at the PL opening.

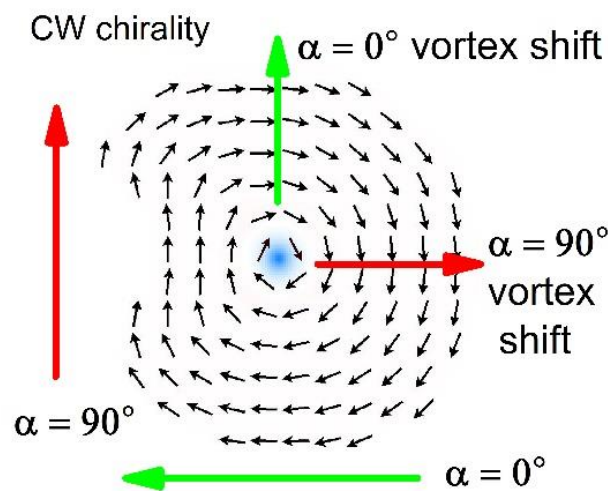


Figure 4-16 Vortex core shift initialized by an applied magnetic field for the CW chirality. Application of a field parallel to the symmetry axis (outside green arrow) shifts the vortex from the central position upwards (inner green arrow). Application of a field at the angle $\alpha = 90^\circ$ with respect to the symmetry axis (outside red arrow) shifts the vortex to the right side, opposite to the opening side (inner red arrow).

In the Figure 4-16 we can see that the vortex shift is perpendicular to the field direction. It applies to both chirality orientations and thus the vortex shifts in the opposite direction either when the magnetisation is curled in the CCW orientation (CW is set in the Figure 4-16) or for the opposite field direction. In other words, we can change the vortex shift direction by selecting the appropriate sequence of the field sweeping.

The last part of the thesis deals with the temperature dependence of the vortex nucleation field. In this part, we have examined different field angles with the aim to find the role of the magnetic state in the SD-V transitions. Since the magnetic states immediately before the vortex annihilation are very similar (vortex state), we have focused only on the entering process of the magnetic vortex.

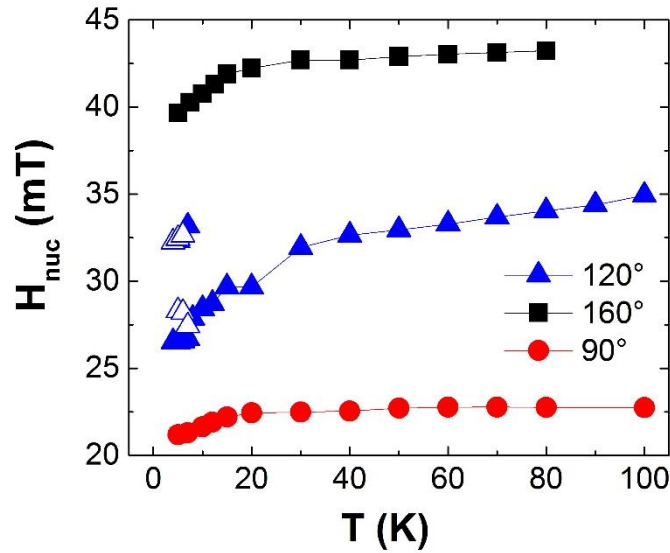


Figure 4-17 Temperature dependence of H_{nuc} for three angles of an applied magnetic field. Slope of each curve differs for $T < 20$ K and $T > 20$ K. Two values of H_{nuc} are possible for 120° field angle and $T < 8$ K.

Each point in the Figure 4-17 is a mean value of at least eight measurements of the magnetisation reversals, positive as well as negative branches. We can also say that the measured values are distributed within the interval ± 0.5 mT, and typical standard deviation is ~ 0.15 mT. One can see that the curves include two remarkable inclinations. The idea of this experiment is based on a publication in Ref. [14], where the authors studied the temperature dependence of the magnetisation reversal in individual submicron Permalloy disks. In their experiment, the dependences also exhibited a non-monotonic behaviour and, furthermore, with positive and negative slopes at low and high temperatures, respectively. They suggested that at low temperatures the vortex nucleation proceeds via thermal activation over an energy barrier, while at high temperatures it is governed by a temperature dependence of the saturation magnetisation. We have decided to perform similar experiments with our modified nanomagnet.

The curves in the Figure 4-17 show two basic slopes – steep and mild for temperatures below and above 20 K, respectively. We assume that the large slopes are caused by presence of many shallow minima of the total energy function due to edge corrugations as well as a granular structure of the Permalloy. At low temperatures, the system has to overcome many small barriers that represent obstacles in magnetisation dynamics. It then contributes significantly to the final nucleation time and in the graph we can see a rapid decrease of the nucleation field. There is a different situation at higher temperatures, the small barriers do not further constitute obstacles due to the thermal energy of the individual magnetic moments, and only the last barrier represents an obstacle for the nucleation. This might therefore decisively reduce the influence of surface roughness on the reversal process. Overcoming the last barrier means that the magnetic vortex enters the object and the energy of the system lowers significantly.

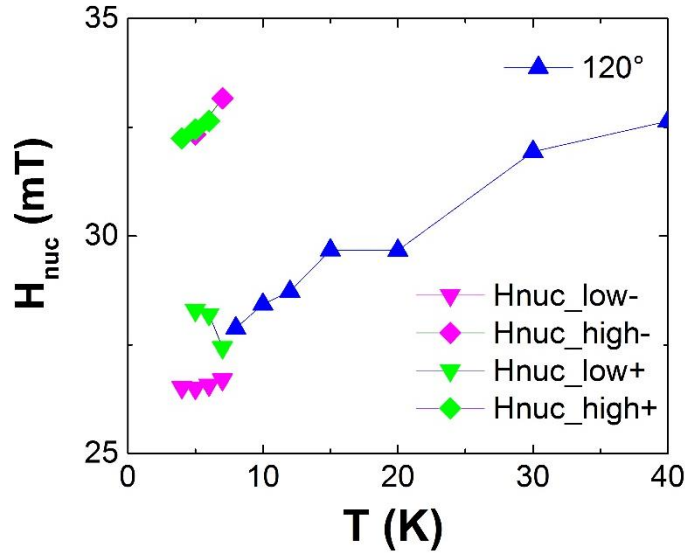


Figure 4-18 Temperature dependence of H_{nuc} for the field angle of 120° and $T < 40$ K. Different H_{nuc} values at the lowest temperatures.

Even though we have tried to choose “stable“ field angles, it is not the case of 120° field angle at very low temperatures ($T < 8$ K). The curve in the Figure 4-18 shows two metastable states in which the system can be trapped. Since we initially did not understand the appearance of the two states, we have analysed the height of the abrupt changes in the Hall voltage that are connected with the vortex nucleation. We have found out that the heights of the voltage jumps clearly depend on the vortex nucleation field. Normally, a point has been calculated as $((H_{\text{nuc}}$ in the positive branch) + $(H_{\text{nuc}}$ in the negative branch))/2, since these two values have been very similar. In this case, if we focus, for example, on the temperature of 5 K, we will get four different values (Figure 4-18). For the positive branch of the loop and the vortex nucleation field $H_{\text{nuc}} = 28$ mT and $H_{\text{nuc}} = 32$ mT, the voltage jumps are $4.5 \pm 0.1 \mu\text{V}$ ($H_{\text{nuc_low+}}$) and $3.8 \pm 0.4 \mu\text{V}$ ($H_{\text{nuc_high+}}$), respectively. The height of the nucleation jumps in the negative branch is $3.9 \pm 0.2 \mu\text{V}$ ($H_{\text{nuc_low-}}$) and $2.9 \pm 0.25 \mu\text{V}$ ($H_{\text{nuc_high-}}$). Based on our previous simulations, a difference of $\sim 25\%$ in the Hall signal can be explained by the two chiralities of the nanomagnet (CW or CCW).

To summarize, in this chapter we have utilized micro-Hall probes to investigate magnetic states in micron and submicron Py ferromagnets.

In our experiments we have used Permalloy thanks to its very low magnetocrystalline anisotropy that we consider equal to zero. Its high magnetic permeability and low coercivity also make this soft magnetic material preferred to use in our study.

Micro-Hall magnetometry is a sensitive technique used for non-invasive observation of magnetic states in patterned magnetic objects. Although this technique has a few drawbacks including, for example, lower spatial resolution, it is still a promising method to study magnetisation reversal in an individual submicron ferromagnet. Simple technology of the Hall probes makes the whole observation easier in comparison with other techniques and it also allows the modification of the Hall probe properties based on our requirements.

Designed Pacman-like ferromagnet with broken shape symmetry allows the study of its magnetic properties much easier as compared to a disk. At first, we have investigated experimentally ferromagnets at the microscopic scale (diameter of $1 \mu\text{m}$) with the conclusion that various magnetic states are observed.

Afterwards, we have gradually reduced dimensions of the PL objects down to 300 nm. As we have examined angular dependences of the vortex nucleation fields in such miniaturized objects in simulations, we could define various distinct pre-nucleation configurations of the magnetic state.

Based on our calculations we have chosen three directions of an applied magnetic field while each of them represent different configuration of local magnetisation in the object just before the vortex nucleation. For the angle of 90° between the PL symmetry axis and an external field, C-state occurs. For field angles of 120° and 160° are magnetic spins arranged to S-state and 2S-state, respectively. Taking into account that these situations are robust, we have shown that the nucleated vortex state from the C-state has opposite chirality as compared to S-state. In addition, vortices created from S-state and 2S-state differ in polarity. While the chirality contribution is sufficient for recording, the signal from vortex polarity is almost ten times smaller and thus it is on the noise level in our experiments.

Further, we have shown how the vortex chirality can be control for certain temperature and field angle by a specific field sequence. In this case we have tested the field angle of 90° where magnetisation reversal curves measured in the asymmetrically shaped ferromagnet have revealed two different values of the vortex annihilation field. This difference has been caused by the vortex annihilation direction, whether the vortex has been expelled to the PL opening or to the opposite side.

Temperature dependence of the vortex nucleation field has been measured to find the role of the magnetic state in the single-domain to vortex-state transition. Three chosen field angles have been investigated in the temperature range of 5 K – 100 K. All three curves have shown two basic slopes – steeper for temperatures lower than 20 K and small slope above 20 K. We assume that at low temperatures all small barriers, originating from edge corrugations and Py grains, represent an obstacle for magnetisation dynamics. In other words, a system at lower temperatures has to overcome many barriers and thus the vortex nucleation takes longer. At higher temperatures the thermal energy helps the system to suppress small barriers, while only the last dominant barrier represents an obstacle for the vortex nucleation. Overcoming the last barrier the system lowers its energy significantly resulting in the vortex state formation

5 Conclusions

It is obvious, also from this work, that the future of the magnetic data storage and memory technology is concerned with squeezing information into smaller and smaller bits and manipulating these bits faster and faster. Controlled manipulation of magnetic domains and vortices in ferromagnetic nanostructures have opened opportunities for novel fast, high-density, and low-power memories, including race track memories, magnetic random access memories, bit patterned media, and skyrmion memories. Up-to-date magnetic systems respond to external magnetic field pulses on the nanosecond time-scale. The main challenge in magnetism today is to develop new methods of magnetisation control on the nanometer scale and the picosecond or even femtosecond time scale. These efforts involve conventional magnetic materials such as transition metals and rare earths, and also novel semiconductor materials.

The work in the thesis presents basic research in the field of micro- and nano-magnetism focused on magnetic particles. Since a controlled manipulation of magnetic domains and vortices in such particles is required, many theoretical and experimental works have been performed recently to understand magnetisation reversal and vortex dynamics in submicron ferromagnetic disks. However, it is difficult to control vortex properties of the disks due to their high degree of symmetry.

The integration of asymmetric ferromagnets complicates the Hall voltage interpretation as compared with highly symmetric object, since the object shape and both, the vortex polarity and chirality can influence the Hall signal significantly. On the other hand, the shape asymmetry can help us to observe magnetic behaviour in detail. In order to support our interpretation of the results obtained, we have combined the Hall probe measurements with micromagnetic simulations in this work.

Based on our simulations we have also find the regime of the PL nanomagnet operation in which the final vortex state is independent on a weak disturbing external field (PL objects < 100 nm). This is a promising finding to consider if using the PL nanomagnet, with a magnetic vortex of a desired polarity and chirality, as a memory element. In previous calculations it has also been carried out that much more complicated situation with nucleation of several vortices appears for large objects (> 500 nm). Therefore, all our effort has been concentrated on the fabrication of a 300-nm PL ferromagnet, for which a simple magnetic state with one vortex should appear, and still reasonable large Hall voltage signal is obtained.

We have studied vortex nucleation and annihilation processes and their temperature dependences in Pacman-like nano-objects using micro-Hall probe magnetometry. Chirality of the object can be easily controlled due to its lowered symmetry. We have shown experimentally that vortex nucleation field strongly depends on the angle of an external in-plane magnetic field. The experiments also confirm that the vortex nucleation proceeds via thermal activation over an energy barrier or few barriers.

6 Záver

Taktiež z tejto práce je jasné, že budúcnosť pamäťových technológií a magnetického ukladania dát súvisí so zhusťovaním zápisu do stále menšieho objemu a s rýchlejšími procesmi záznamu. Kontrolované ovládanie magnetických domén a magnetických vírov vo feromagnetických nanoštruktúrach umožňuje vývoj nových, rýchlych pamätí s vysokou hustotou zápisu a nízkou spotrebou, medzi ktoré patria napríklad takzvané “race track” pamäte, magnetické pamäte s náhodným prístupom alebo najnovšie pamäte využívajúce skyrmiony ako nosiče informácií. Odozva dnešných pamätí na externé magnetické pulzy je na úrovni nano-sekúnd. Hlavnou výzvou tejto oblasti je vývoj nových metód, pomocou ktorých by bolo možné nastavovať magnetické stavy na úrovni nanometrov s piko-sekundovými alebo až femto-sekundovými rýchlosťami. Toto úsilie tiež zahŕňa vývoj nových jedinečných polovodičových materiálov.

Prezentovaná práca sa zaoberá základným výskumom v oblasti mikro- a nano-magnetizmu zameraného prednostne na magnetické prvky. Mnoho prác v súčasnej dobe pojednáva o vyšetrowaní magnetických stavov a dejov vo feromagnetických útvaroch s rozmermi menšími ako 1 μm . Prevažne však ide o symetrické útvary, ktorých vlastnosti ako sú napríklad preklopenie magnetizácie alebo dynamika magnetického víru sa vyšetrujú komplikovane, prípadne nejednoznačne.

I keď využitie asymetrických feromagnetov môže skresľovať interpretáciu nameraného signálu, keďže dochádza napríklad ku zmiešavaniu príspevkov od polarity a chiraloty objektu, práve asymetrický tvar by mal napomáhať k podrobnému sledovaniu magnetických vlastností. Ďalšou podporou je použitie mikromagnetických simulačných prostredí na koreláciu so získanými experimentálnymi údajmi.

Pomocou simulácií bol tiež zistený optimálny režim PL nanomagnetu, pri ktorom je magnetický vír v stabilnom stave, nezávislom od slabých vonkajších polí (PL útvary menšie ako 100 nm). Definovanie stavu s požadovanou chiralitou a polaritou je základným predpokladom pre využitie PL feromagnetov ako pamäťových buniek. Z predošlých simulácií tiež vyplýva, že situácia v objektoch väčších ako 500 nm je omnoho zložitejšia, keďže dochádza k formácii rôznych nedefinovatelných magnetických stavov. Preto sme sa v našej práci zamerali hlavne na technológiu a vyšetrowanie vlastností 300 nanometrových PL útvarov, v ktorých by mal byť definovaný stav s jedným magnetickým vírom a zároveň by nám naša cilitivá mikro-Hall magnetometria umožňovala pozorovať deje v rámci týchto štruktúr.

Cieľom práce bolo pozorovať a vyhodnotiť procesy nukleácie a anihilácie magnetických vírov vo feromagnetických PL nanomagnetoch. Vďaka teplotným a uhlovým závislostiam sme boli schopní kontrolovať smer rotácie magnetizácie v rovine objektov so zníženou symetriou. Experimentálne sme ukázali, že hodnota magnetického poľa, pri ktorom vniká magnetický vír je výrazne závislá od smeru pôsobiaceho vonkajšieho poľa. Experimenty tiež potvrdzujú, že vniknutie magnetického víru do objektu prebieha formou tepelnej aktivácie cez energetickú bariéru, prípadne mnohonásobné bariéry.

7 Publications and Presentations

Published Papers

Ščepka, T., Polakovič, T., Šoltýs, J., Tóbik, J., Kulich, M., Kúdela, R., Dérer, J., and Cambel, V., Individual vortex nucleation/annihilation in ferromagnetic nanodots with broken symmetry observed by micro-Hall magnetometry. *AIP Advances* 5, 117205 (2015)

Ščepka, T., Šoltýs, J., Precner, M., Fedor, J., Tóbik, J., Gregušová, D., Gucmann, F., Kúdela, R., Cambel, V., Vortex dynamics in ferromagnetic nanoelements observed by micro-hall probes. *Acta Phys. Polonica A* 126 (2014) 390-391.

Cambel, V., Precner, M., Fedor, J., Šoltýs, J., Tóbik, J., **Ščepka, T.**, Karapetrov, G., High resolution switching magnetization magnetic force microscopy. *Applied Phys. Lett.* 102 (2013) 062405.

Ščepka, T., Gregušová, D., Gaži, Š., Haščík, Š., Fedor, J., Šoltýs, J., Kúdela, R., Cambel, V., : Detection elements for on-cantilever laboratory. In: ASDAM 2012. Eds. Š. Haščík, J. Osvald. Piscataway: IEEE 2012. ISBN 978-1-4673-1195-3. P. 91-94.

Kúdela, R., Gregušová, D., **Ščepka, T.**, Eliáš, P., Gaži, Š., MOVPE grown InGaP/(Al, Ga)As free standing structures. In: EW-MOVPE XIV. Ed. J. Prazmowska. Wroclaw: House of Wroclaw Univ. Technol. 2011. ISBN 978-83-7493-599-9. P. 57-61.

Presentations

“Magnetization reversal of ferromagnetic nanoelements observed by micro-Hall probe magnetometry”, RTNSA '15 - Recent Trends in Nanomagnetism, Spintronics and their Applications, July 2015, Ordizia, Spain (poster).

“Magnetization reversal of ferromagnetic nanoelements observed by micro-Hall probe magnetometry”, Nanomaterials MSnows '14, September 2014, Nancy, France (poster).

“Vortex Dynamics in Ferromagnetic Nanoelements Observed by Micro-Hall Probes”, CSMAG'13 – 15th Czech and Slovak Conference on Magnetism, June 2013, Košice, Slovakia (oral).

“Technology of microcantilevers with integrated field-effect-transistors as sensing elements”, 15th School of Vacuum Technology, November 2012, Štrbské Pleso, High Tatras, Slovakia (oral).

“Detection elements for on-cantilever laboratory”, ASDAM '12 - The Ninth International Conference on Advanced Semiconductor Devices and Microsystems, November 2012, Smolenice, Slovakia (oral).

“Technology and testing the mechanical properties of the InGaP/GaAs/InGaP microcantilevers”, 40th Conference on the Physics of Semiconductors „Jaszowiec“, June 2011, Krynica-Zdrój, Poland (poster).

Others

Cambel, V., Tóbik, J., Ščepka, T., Polakovič, T., Precner, M., Fedor, J., and Šoltýs, J., Vortex dynamics in ferromagnetic nanodots with broken symmetry, MSnows 2014, Nancy, France (poster).

8 References

- [1] R. P. Cowburn, D. K. Koltsov, A. O. Adeyeye, M. E. Welland a D. M. Tricker, „Single-Domain Circular Nanomagnets,“ *Phys. Rev. Lett.*, vol. 83, no. 1042, 1999.
- [2] G. Gubbiotti, G. Carlotti, F. Nizzoli, R. Zivieri, T. Okuno a T. Shinjo, „Magnetic Properties of Submicron Circular Permalloy Dots,“ *IEEE Trans. Magn.*, vol. 38, no. 5, 2002.
- [3] R. Pulwey, M. Rahm, J. Biberger a D. Weiss, „Switching behavior of vortex structures in nanodisks,“ *IEEE Trans. Magn.*, vol. 37, no. 2076, 2001.
- [4] A. K. Geim, S. V. Dubonos, J. G. S. Lok, I. V. Grigorieva, J. C. Maan, L. Theil Hansen a P. E. Lindelof, „Ballistic Hall micromagnetometry,“ *Appl. Phys. Lett.*, vol. 71, no. 2379, 1997.
- [5] J. G. S. Lok, A. K. Geim, J. C. Maan, S. V. Dubonos, L. Theil Kuhn a P. E. Lindelof, „Memory effects in individual submicrometer ferromagnets,“ *Phys. Rev. B*, vol. 58, no. 18, 1998.
- [6] T. M. Hengstmann, D. Grundler, C. Heyn a D. Heitmann, „Stray-field investigation on permalloy nanodisks,“ *J. Appl. Phys.*, vol. 90, no. 12, 2001.
- [7] M. Rahm, M. Schneider, J. Biberger, R. Pulwey, J. Zweck, D. Weiss a V. Umansky, „Vortex nucleation in submicrometer ferromagnetic disks,“ *Appl. Phys. Lett.*, vol. 82, no. 23, 2003.
- [8] M. Schneider, H. Hoffmann, S. Otto, T. Haug a J. Zweck, *J. Appl. Phys.*, vol. 92, no. 1466, 2002.
- [9] Zhong, Zhiyong, Zhang, Huaiwu, Jing, Yulang, Tang, Ke a Liu, Shuang, „Micromagnetic simulation of magnetization reversal in submicron dots with laterally gradient magnetization,“ *J. Magn. Magn. Mater.*, vol. 314, no. 1, pp. 43-46, 2007.
- [10] Yan Liu a An Du, „Arrangement effects of triangular defects on magnetization reversal process,“ *J. Magn. Magn. Mater.*, vol. 323, pp. 461-464, 2011.
- [11] J. Li, J. Shi a S. Tehrani, „Temperature-Dependent Switching Properties in Patterned 200nm NiFe Structures,“ *Appl. Phys. Lett.*, vol. 79, no. 3821, 2001.
- [12] R. K. Dumas, K. Liu, C.-P. Li, I. V. Roshchin a I. K. Schuller, „Temperature induced single domain – vortex state transition in sub-100nm Fe nanodots,“ *Appl. Phys. Lett.*, vol. 91, no. 202501, 2007.
- [13] H. Shima, V. Novosad, Y. Otani, K. Fukamichi, N. Kikuchi a O. Shimada, „Pinning of magnetic vortex in microfabricated permalloy disk,“ *J. Appl. Phys.*, vol. 92, no. 1473-7, 2002.
- [14] G. Mihajlović, M. S. Patrick, J. E. Pearson, V. Novosad, S. D. Bader, M. Field, G. J. Sullivan a A. Hoffmann, „Temperature dependent nucleation and annihilation of individual magnetic vortices,“ *Appl. Phys. rev.*, vol. 96, no. 112501, 2010.
- [15] A. Oral, S. J. Bending a M. Henini, „Real-time scanning Hall probe microscopy,“ *Appl. Phys. Lett.*, vol. 69, no. 9, pp. 1324-1326, 1996.
- [16] M. Murakami, K. D. Childs, J. M. Baker a A. Callegari, „Microstructure studies of AuNiGe Ohmic contacts to n-type GaAs,“ *J. Vac. Sci. Technol. B*, vol. 4, no. 903, 1986.
- [17] V. Cambel a G. Karapetrov, „Control of vortex chirality and polarity in magnetic nanodots with broken rotational symmetry,“ *Phys. Rev. B*, vol. 84, no. 014424, 2011.